HHS Public Access

Author manuscript

Magn Reson Imaging. Author manuscript; available in PMC 2017 April 01.

Published in final edited form as:

Magn Reson Imaging. 2016 April ; 34(3): 280–288. doi:10.1016/j.mri.2015.10.034.

Improved receiver arrays and optimized parallel imaging accelerations applied to time-resolved 3D fluoroscopically tracked peripheral runoff CE-MRA

Paul T. Weavers, PhD[a], **Eric A. Borisch, MS**[a], **Tom C. Hulshizer, BS**[a], **Phillip J. Rossman, MS**[a], **Phillip M. Young, MD**[b], **Casey P. Johnson, PhD**[c], **Jessica McKay, BS**[c], **Christopher C. Cline, BS**[c], and **Stephen J. Riederer, PhD**[a]

[a]Mayo Clinic MR Laboratory, 200 First Street Southwest, Rochester, Minnesota, 55905

[b]Department of Radiology, 200 First Street Southwest, Rochester, Minnesota, 55905

[c]University of Minnesota, 1200 Washington Ave S, Minneapolis, Minnesota 55415-1227

Abstract

Objectives—Three-station stepping-table time-resolved 3D contrast-enhanced magnetic resonance angiography has conflicting demands in the need to limit acquisition time in proximal stations to match the speed of the advancing contrast bolus and in the distal-most station to avoid venous contamination while still providing clinically useful spatial resolution. This work describes improved receiver coil arrays which address this issue by allowing increased acceleration factors, providing increased spatial resolution per unit time.

Materials and Methods—Receiver coil arrays were constructed for each station (pelvis, thigh, calf) and then integrated into a 48-element array for three-station peripheral CE-MRA. Coil element sizes and array configurations for these three stations were designed to improve SENSE-type parallel imaging taking advantage of an increase in coil count for all stations versus the previous 32 channel capability. At each station either Acceleration Apportionment or optimal CAIPIRINHA selection was used to choose the optimum acceleration parameters for each subject. Results were evaluated in both single- and multistation studies.

Results—Single-station studies showed that SENSE acceleration in the thigh station could be readily increased from R = 8 to R = 10, allowing reduction of the frame time from 2.5 to 2.1 sec to better image the typically rapidly advancing bolus at this station. Similarly, the improved coil array for the calf station permitted acceleration increase from R = 8 to R = 12, providing a 4.0 vs. 5.2 sec frame time. Results in three-station studies suggest an improved ability to track the contrast bolus in peripheral CE-MRA.

Corresponding Author. Paul T. Weavers, MR Laboratory, 200 First Street SW, Rochester, MN 55906, FAX: 507-538-3946, OFFICE: 507-534-9780, weavers.paul@mayo.edu.

Conclusions—Modified receiver coil arrays and individualized parameter optimization have been used to provide improved acceleration at all stations in multi-station peripheral CE-MRA and provide high spatial resolution with frame times as short as 2.1 sec.

1. Introduction

Bolus-chase three-dimensional (3D) contrast-enhanced magnetic resonance angiography (CE-MRA) has been demonstrated as a useful method for visualizing the entirety of the vasculature of the lower periphery [1–6]. A variety of approaches have been employed to provide good performance in visualizing the arterial vasculature in peripheral CE-MRA, including single-injection multi-station stepping table MRA [7,8], continuously moving table bolus tracking [9], and use of multiple injections for separate anatomic stations [10,11]. Although the development of receiver arrays with high parallel imaging performance may benefit many areas of magnetic resonance imaging (MRI), the unique technical demands of single-injection fluoroscopic tracking multi-station CE-MRA will be highlighted in this work.

A fundamental limitation in multi-station peripheral CE-MRA is that the acquisition time in a proximal station must be long enough to enable sufficient spatial resolution in that station while still being short enough to allow for table movement to capture the arterial phase at the next station. This is more stringent than in single-station exams in which an elliptical-centric phase encoding order [12,13] allows long (>20 sec) acquisition times with good venous suppression. Such extensive times are not feasible for the proximal stations in single-injection multi-station CE-MRA. Although compression cuffs can be used to delay the onset of venous enhancement [14,15], this requires additional setup time. Also, any improvement in proximal station spatial resolution must largely be done by increasing the rate at which k-space is traversed.

A primary means to more rapidly traverse k-space is parallel imaging, such as Sensitivity Encoding (SENSE) [16,17] or Generalized Auto-calibrating Partially Parallel Acquisition (GRAPPA) [18]. Parallel imaging allows an increased rate of sampling of the phase encode directions of k-space but is dependent upon the suitability of the multi-element phased array receiver [19]. Vendors are now providing high channel count receiver arrays, but the GEM suite peripheral vascular array for example (GE Healthcare, Waukeshau, Wisconsin) is limited to a maximum SENSE acceleration of 6. Previous work in time-resolved 3D CE-MRA of the calves used receiver coil arrays comprised of up to eight elements attached together in a linear array and wrapped around the anatomic region circumferentially. This allowed 2D parallel acquisition along the two transverse phase-encoding directions, anterior/posterior (A/P) and left/right (L/R), with acceleration factors as high as R = 8 routinely used [6,7,20–24]. One aspect of this current work was to investigate adaptation of this circumferential design to the station-specific anatomy, possibly with increased coil count, for higher acceleration.

With 2D acceleration factors of R = 4 or more, there can begin to be uncertainty in how to best achieve this acceleration. For example, R can be differentially apportioned along the two phase encode directions [25] or alternative undersampling patterns such as Controlled

Aliasing In Parallel Imaging Results IN Higher Acceleration (CAIPIRINHA) [26,27] can be applied. It has been shown that optimization of the acceleration apportionment or the CAIPIRINHA sampling pattern can be advantageous for 3D CE-MRA for $R \geq 8$ [25,27]. Moreover, the optimization can be performed prior to the actual contrast-enhanced scan and is fast enough to allow practical implementation on a patient-specific basis [25]. The optimization tailors the specific k-space undersampling pattern to the coil array used, its positioning on the body, and the body habitus of the subject.

A recent development in multi-station CE-MRA has been the technique of fluoroscopic tracking [7,8,21], a method which provides real-time imaging at all stations and allows the operator to interactively control the movement of the table from one station to the next in synchrony with the advancing contrast bolus. This method eliminates the need for a test bolus or a repeat injection for the calf station. Initial results were obtained without the benefit of the aforementioned acceleration optimization techniques. Also, as known from other studies [28], the initial results showed that in the thigh station in particular the transit of the contrast bolus was so fast that frame times less than the 2.5 sec used would be desirable to more accurately track contrast advance. The synergistic combination of better-performing receiver arrays and acceleration optimization techniques can potentially reduce frame times while maintaining spatial resolution and image quality.

The purpose of this work is to describe how further advances in the design and application of multi-element receiver coils, coupled with 2D parallel imaging optimization, can be applied to drive down the frame times of three-station time-resolved bolus-chase CE-MRA with fluoroscopic tracking. In the following sections we describe how the individual coil arrays were modified at each station, present results for each station acquired individually, and then describe how the modified arrays were integrated into a multi-station peripheral CE-MRA protocol utilizing fluoroscopic tracking.

2. Materials and Methods

2.1 Overall receiver coil design considerations

At each of the three stations (pelvis, thighs, and calves) the receiver coil array was designed to: (i) fit a wide variety of patient body habitus at that station, (ii) minimize g-factors for improved SENSE performance, (iii)work either on its own for imaging that station exclusively or for integration into a full three-array system for multi-station imaging, (iv) minimize coil sensitivity falloff near the S/I edges of each station, and (v) be subject to an overall 48-channel limit on our MRI scanner for three-station imaging. The latter is an increase over the 32-channel limit previously available in Ref. [8].

The general design process utilized linear circumferential receiver arrays that have been previously reported for multiple anatomic regions [7,20,29–31]. Peripheral 3D CE-MRA is generally performed with frequency encoding along the superior-inferior (S/I) direction. Because acceleration is not performed along the S/I direction, each individual element length was sized according to the full S/I coverage desired. The width was determined by the predicted circumference divided by the number of elements available. The configuration of each element, specifically its size and the distance between it and the anatomy to be

imaged, as well as the configuration of each element relative to its neighbor was then refined by experiments and simulations utilizing the g-factor. That is, each array was prototyped with a set of identical coil elements which had not yet been fixed together. The pelvis and thigh coil arrays were designed to be comprised of multiple two-element modules, with the number of modules selected and connected together to match the patient-specific body habitus at that station. The final design should exhibit high signal-to-noise ratio (SNR) and low g-factor noise to facilitate maximum parallel imaging performance.

2.2 Calf receiver coil design

Previous work to image lower periphery with eight coil elements and acceleration apportionment with R = 9.67 suggested that higher acceleration factors would still have adequate SNR to visualize small vessels [32]. Desire for further increased acceleration levels led to consideration of a major increase in coil count. The design was specified to accommodate an FOV with approximately 40 cm S/I coverage and full bilateral coverage transversely. Because there is typically less patient-to-patient variability in the field-of-view (FOV) in the calves than, say, the abdomen, the coil count was fixed at 16 and the array was designed to accommodate virtually all subjects. Receiver elements were constructed to be rectangles of 40 cm × 7.8 cm compared to 27 cm × 14.4 cm and 27 cm × 10.5 cm of the previous calf array, a comparison shown in Figure 1.

Next, multiple elements were fabricated and the positioning of the elements was evaluated via g-factor calculations at hypothetical SENSE accelerations investigating trade-offs in proximity to tissue, individual receiver element overlap, and positioning of the anatomy within the receiver array and evaluated by an SNR unit reconstruction [33]. Experiments involving spacing between the legs, angling the coils between the legs, and fixing receiver array radius versus allowing non-ideal coil overlap were also investigated as shown in Figure 2 [34]. Panels (a,b), show how angling the center elements towards the calves (b) improves the g-factor response (cooler colors) vs. no angling (a). Panels (c,d), show how spacing the legs apart from each other slightly (d) also improves g-factor response for this fixed FOV that encompassed the entirety of the calves in the L/R direction. Panels (e,f), show that given a calf size which does not fully fill the receiver array, it is better to ensure each element is as close to the tissue as possible (f) vs. maintaining the circumferential spacing of elements in the array to minimize mutual inductance (e). To this end, a rigid six-coil paddle is attached to two-element flexible wings as the underside of the array, and another rigid six-coil paddle is placed on top of the patient to complete the circumferential coverage. The result of this is a design which can be appreciated in Figure 1b, a 16 element receiver with long, thin elements running S/I, angled center elements both to minimize distance to tissue and to space the legs slightly apart. In this figure, elements 1–6 comprise the anterior paddle described above.

2.3 Thigh receiver coil design

To increase the acceleration factor in the thigh station a greater number of elements than the ten used previously was considered essential. Additionally, to preserve SNR the thigh coil redesign was undertaken with the goal of minimizing the receiver coil-to-tissue air gap along the length of the S/I FOV with knowledge of a general taper in circumference of body

habitus from hip to knee as can be visualized in Figure 3. To that end measurements from previously acquired 3D image sets of 20 subjects were analyzed to determine a representative taper angle from the hips to the knees, the proposed coverage regime for this receiver array. A taper angle of 10 degrees was found to accommodate the change in body width at the level of the hips versus the knees for all cases. With this accommodation angle estimated, trapezoidal receiver elements were then fabricated such that the entire array tapered at a more conservative 7.8 degree angle to provide complete circumferential coverage for a wide range of patient sizes. The width of an individual coil element at the superior end was reduced from the 12 cm used previously to 9.5 cm with the new design. This is evident in Figure 3 (a) versus (b), in which the previous array has a uniform width of 45 cm, but the newer array is narrowed down to 39 cm at the inferior end. With the slight taper the width at the inferior end of each element was 8 cm. The coil element length was 40 cm. Two-element modules were then constructed using the tapered elements. With this redesign, 14 elements are typically used in smaller patients (BMI < 30, as shown in Figure 3), and 16 elements for larger patients. These coil counts are higher than the 10 elements typically used previously. The specific number of modules can be easily selected at the time of the MRI exam.

2.4 Pelvis receiver coil design

Unlike the calves or thighs, the pelvis does not have a unique geometrical shape to take advantage of for array design. A two-element module with slightly narrower elements (12.1 vs. 7.5 cm) was constructed, increasing the coil element count from 12 of the earlier design [8] to typically 14 to 16 with the new array.

2.5 Parallel imaging prescription

Fluoroscopic tracking is sensitive to the acquisition parameters used to acquire each station [8,35]: if one dwells too long at the proximal stations then the distal stations suffer from venous overlay on the arterial frames. If one spends too little time at the proximal stations, there may not be enough information to clearly follow the course of a given artery. Table 1 shows the fluoroscopic tracking protocol as used in Ref. [8], and also details the improvements afforded by the new receiver coils and parallel imaging technique. Each of three imaging stations (pelvis, thighs, and calves) to be used for fluoroscopic tracking technique was analyzed offline to first determine which strategy, Acceleration Apportionment or optimal CAIPIRINHA, would be utilized for SENSE acceleration optimization, the analysis done using a method described previously [25,27]. For both techniques the optimum acceleration is determined with analysis of the g-factor, a mathematical description of the noise amplification introduced by SENSE acceleration [16], as a predictor of image quality. For each station a set of 10 representative, previously archived studies was selected, and for each of these the coil calibration images from receiver arrays comprised of eight or more elements were available. The coil calibration data allows calculation of the g-factor maps of each station with hypothetical accelerations applied [16]. Coil calibration data for each station were tested with acceleration factors ranging from R = 4 to 12 in the case of the pelvis and thigh stations, and R = 8 to 16 in the case of the calf station. It was found that Acceleration Apportionment consistently suited the calf station at

R = 12, and optimal CAIPIRINHA was better compatible with the thigh (R = 10) and pelvis (R = 8) stations.

2.6 General in-vivo methods

The new coil arrays were evaluated using in vivo studies performed in a total of 19 volunteers (ages 19–55 years, weight 135–256 pounds, 9 female). Each volunteer was enrolled under an IRBapproved protocol and provided written informed consent. Images were acquired on a 3.0T GE MRI scanner (Waukesha, Wisconsin, USA). An injection of 20 mL of gadobenate dimeglumine (MultiHance, Bracco, Princeton N.J., USA) contrast agent was administered via power injector into an arm vein followed by 20 mL of saline flush at 3 mL/s for each exam. In several instances volunteers were imaged in two sessions separated by at least 24 hours to allow contrast clearance.

2.7 In-vivo single station evaluation

Comparisons utilizing highly-accelerated time-resolved CE-MRA between the previous and redesigned coil arrays in individual stations were accomplished with a view-shared sequence [29]. In general the spatial resolution was kept constant between the scans using the previous and new coils, and any increase in acceleration was used to reduce acquisition time for the same resolution. Sequence parameters for each station for the previous and new methods are shown in Table 1.

2.8 In-vivo three-station evaluation

The three redesigned coils for the pelvis, thighs, and calves were then integrated into an extended array and evaluated using the real-time fluoroscopic tracking protocol developed by Johnson et al. [8], but modified for the receivers' greater capabilities. Details are shown in Table 1 with each station utilizing identical parameters as the single-station "new" parameters, but with real-time fluoroscopic tracking enabled. The previous protocol at the pelvic, thigh, and calf-foot stations was able to provide a 3D image every 2.5, 2.5, and 5.25 seconds, respectively. Combined with patient-specific acceleration parameters, the new receiver array enabled update times of 2.5, 2.1, and 4.0 seconds, respectively with no degradation in spatial resolution.

3. Results

We compared the new and old receiver arrays in single-station targeted CE-MRA studies, with a representative example shown in Figure 4 for the thighs. Panels (a) and (b) show comparable coronal MIPs from two volunteers, (a) acquired at R = 8 acceleration, and (b) acquired at R = 10 acceleration with a modified CAIPIRINHA undersampling pattern [27], in this case 1 × 10 (7), where this nomenclature represents the $R_Y \times R_Z$ (CAIPIRINHA shift) as described in Ref. [26]. Note again reduced noise amplification in the g-factor comparison (c) in the redesigned (b) vs. the previous (a) coil. Also note the spacing between the knees in panel (b) due to the desire to integrate this into a three-station configuration in which the inferior aspect of the thigh coil abuts the superior aspect of the new 16-channel calf array, which spaces the calves by design.

Moving down the body, Figure 5 compares a representative calf comparison utilizing the optimized accelerations and new receiver array. Full FOV coronal maximum intensity projections (MIPs) are shown for a CE-MRA study done with acceleration factor R=8 ($R_Y \times R_Z = 4 \times 2 = 8$) with the previous eight-element coil (a) and for a second study done at R=12 ($R_Y \times R_Z = 6 \times 2 = 12$) with the redesigned 16-element coil (b). A comparison of the whole-volume g-factor is shown in panel (c) for the two cases shown in (a) and (b). Panels (d–h) show a sequence of images of the targeted region of the 8× MIP indicated in (a) at consecutive 5.2 sec frame times, and panels (i–m) show a similar region from the 12× MIP in panel (b) for the 4.0 sec frame times. Note the lower noise amplification in (i–m) vs. (d–h) despite the higher (12× vs. 8×) acceleration.

Using the three new receiver arrays, three-station bolus-chase MR angiograms were acquired using the higher acceleration factors and shorter frame times and temporal footprints as listed in Table 1. Results of one volunteer study are shown in Fig. 6a, which shows a coronal MIP consisting of select time frames from the pelvis, thigh, and calf stations. The MIP consists of the last image acquired from the proximal two stations, and the second image acquired in the calf station. A typical layout of the arrays for the three-station fluoroscopic tracking exam is shown in Fig. 6b.

Results from another subject imaged using three-station acquisition with fluoroscopic tracking are shown in Figure 7. Panel (a) shows a full coronal FOV MIP of another volunteer consisting of one time-resolved frame from each of the three stations. Panels (b,c,d) are the time frames immediately preceding the table motion at the pelvis station in the sub-volume identified in (a). The images show scans of progressively 2.5, 5.0, and 7.5 sec of total acquisition time of the contrast-enhanced blood. Panels (e) and (f) show targeted MIPs for the two time frames of the 3D sub-volume acquired in the thigh station. The images in panels (e) and (f) were formed with only 2.1 and 4.2 sec of acquired data, respectively. There was no time to spend acquiring additional data since the contrast-enhanced blood had reached the distal end of the thigh FOV by time the image in (e) was displayed to the operator. Upon seeing this contrast transit the operator triggered table advance, acquisition of the current frame (f) was completed, and the table was moved. Panels (g,h,i) show the first three frames in the proximal portion of the left calf, demonstrating high arterial quality with negligible venous contamination.

4. Discussion

We have shown how the redesign of multi-element receiver coils and the incorporation of acceleration optimization can potentially improve the performance of multi-station CE-MRA. The principal technical challenge of multi-station CE-MRA is to acquire data for a long enough time at each station to allow adequate spatial resolution but short enough to permit table advance to keep pace with the advancing contrast bolus to avoid venous contamination distally. This is particularly challenging in the thighs, where the contrast bolus traverses rapidly, as well as in the calves, where any delays in table advance at the proximal stations are cumulative and thereby increase the likelihood of venous contamination.

Performing effective parallel imaging with high acceleration factors requires coil arrays with not only sufficient coil count but also with good signal-to-noise ratio. One method for increasing the available parallel imaging acceleration level is simply to increase the number of independent receiver coils elements. This has been taken to extremes as high as 128 elements [36], but practical limits for our application dictate a total element count maximum of 48. Another important consideration in designing receiver arrays to support parallel imaging is to select the positions of the individual array elements to provide a unique falloff in sensitivity along the directions of acceleration [17].

It is important to note that the application of acceleration and the design of the receiver arrays should be considered simultaneously. In the initial description of 2D acceleration, Weiger et.al. [17] noted that the placement of the receiver arrays and the acceleration direction and magnitude had a straightforward relationship with 4 receivers and R = 4. This work extends that idea to much higher acceleration, where it is not as apparent how 16 receivers and an R = 12 acceleration level will best complement each other.

Although the coil array used in the pelvis was also redesigned, the inability to use a defining shape of the anatomy to alter the array in some meaningful way compared to a standard linear circumferential array limited any observed improvement. Also noted is that the percent increase in coil count in the abdomen (12–14 to 16, or about 25%) was smaller than in the thighs (10 to 14–16, 40% or more) and calves (8 to 16, 100%). Aside from the array itself, imaging the pelvis without using breath holding typically introduces motion, another dimension of potential degradation of image quality. Such motion-related artifacts may be mitigated by other methods, such as subtractionless Dixon imaging [37–40].

In the thigh a modified array was developed comprised of slender elements with a slight taper. The increased coil count, typically 14 or 16 elements, arranged in circumferential fashion about the thighs allows 2D-SENSE acceleration with R = 10. The slight taper better matches the coil array to the typically tapered S-to-I surface of the subject at this station. These acceleration levels provide a 2.1 sec frame time and maximum temporal footprint of 5.7 sec at this station for 1.5 mm isotropic resolution. In practice the bolus transit can be rapid enough that only two frames of data are acquired. The cumulative acquisition times for Figures 5e and f were only 2.1 and 4.2 sec, respectively. That is, only one-third and two-thirds of the already highly undersampled k-space were used to form these results. Despite this, image quality is still high due to the short temporal footprint afforded by the high image acceleration [35].

In the calves the overall goal is to again provide high spatial resolution per unit acquisition time, but unlike in the proximal pelvis and thigh stations, a short 2.1 frame time to allow precise triggering of additional table advance is generally not needed. Accordingly, a somewhat longer frame time of 4.0 sec was used, permitting faster buildup of spatial resolution than in the thighs and pelvis. The redesigned coil array with 16 elements permitted 2D-SENSE acceleration of R = 12 which when combined with 2D homodyne acceleration of 1.8 yielded net acceleration R_{NET} = 21.6, permitting 1.0 mm isotropic resolution. In the same vein, if such high temporal resolution imaging is not required in the proximal stations such as in single-station studies, the higher acceleration available with

these arrays and acceleration techniques could be applied to increase spatial resolution to, say, 1.4 mm isotropic with no increase in acquisition time vs. the previous fluoroscopic tracking protocol.

The combination of these three arrays allows for shorter update time and higher spatial resolution per unit time in the CE-MRA of the anatomic regions studied. For fluoroscopic tracking this allows for subjects with faster flow to be successfully imaged without venous overlay on the distal station. Further progress in this direction will allow CE-MRA to be a flexible alternative to CTA, as the station dwell time can be tailored to the individual without the need for a timing bolus [8].

In summary we have shown how receiver coil arrays can be further adapted and combined with acceleration optimization methods to potentially improve the performance of highly-accelerated 3D CE-MRA in single station imaging of the peripheral vasculature while also better enabling fluoroscopically tracked multi-station CE-MRA. 5.

Acknowledgments

Authors acknowledge NIH grants NIH EB000212, HL070620, RR018898 funding this work.

References

1. Ho KY, Leiner T, de Haan MW, Kessels AG, Kitslaar PJ, van Engelshoven JM. Peripheral vascular tree stenoses: evaluation with moving-bed infusion-tracking MR angiography. Radiology. 1998; 206:683–692. [PubMed: 9494486]
2. Meaney JF, Ridgway JP, Chakraverty S, Robertson I, Kessel D, Radjenovic A, et al. Stepping-table gadolinium-enhanced digital subtraction MR angiography of the aorta and lower extremity arteries: preliminary experience. Radiology. 1999; 211:59–67. [PubMed: 10189454]
3. Maki JH, Wilson GJ, Eubank WB, Hoogeveen RM. Utilizing SENSE to achieve lower station sub-millimeter isotropic resolution and minimal venous enhancement in peripheral MR angiography. J Magn Reson Imaging. 2002; 15:484–491. [PubMed: 11948840]
4. Leiner T, Nijenhuis RJ, Maki JH, Lemaire E, Hoogeveen R, van Engelshoven JM. Use of a three-station phased array coil to improve peripheral contrast-enhanced magnetic resonance angiography. J Magn Reson Imaging. 2004; 20:417–425. [PubMed: 15332249]
5. Madhuranthakam AJ, Hu HH, Kruger DG, Glockner JF, Riederer SJ. Contrast-enhanced MR angiography of the peripheral vasculature with a continuously moving table and modified elliptical centric acquisition. Radiology. 2006; 240:222–229. [PubMed: 16793981]
6. Potthast S, Wilson GJ, Wang MS, Maki JH. Peripheral moving-table contrast-enhanced magnetic resonance angiography (CE-MRA) using a prototype 18-channel peripheral vascular coil and scanning parameters optimized to the patient's individual hemodynamics. J Magn Reson Imaging. 2009; 29:1106–1115. [PubMed: 19388111]
7. Johnson CP, Borisch EA, Glockner JF, Young PM, Riederer SJ. Time-resolved dual-station calf–foot three-dimensional bolus chase MR angiography with fluoroscopic tracking. J Magn Reson Imaging. 2012; 36:1168–1178. [PubMed: 22753021]
8. Johnson CP, Weavers PT, Borisch Ea, Grimm RC, Hulshizer TC, LaPlante CC, et al. Three-station three-dimensional bolus-chase MR angiography with real-time fluoroscopic tracking. Radiology. 2014; 272:241–251. [PubMed: 24635676]
9. Madhuranthakam AJ, Kruger DG, Riederer SJ, Glockner JF, Hu HH. Time-resolved 3D contrast-enhanced MRA of an extended FOV using continuous table motion. Magn Reson Med. 2004; 51:568–576. [PubMed: 15004799]

10. Berg F, Bangard C, Bovenschulte H, Nijenhuis M, Hellmich M, Lackner K, et al. Hybrid contrast-enhanced MR angiography of pelvic and lower extremity vasculature at 3.0 T: initial experience. Eur J Radiol. 2009; 70:170–176. [PubMed: 18243622]
11. Attenberger UI, Haneder S, Morelli JN, Diehl SJ, Schoenberg SO, Michaely HJ. Peripheral arterial occlusive disease: evaluation of a high spatial and temporal resolution 3-T MR protocol with a low total dose of gadolinium versus conventional angiography. Radiology. 2010; 257:879–887. [PubMed: 20959539]
12. Wilman AH, Riederer SJ. Performance of an elliptical centric view order for signal enhancement and motion artifact suppression in breath-hold three-dimensional gradient echo imaging. Magn Reson Med. 1997; 38:793–802. [PubMed: 9358454]
13. Willinek WA, Gieseke J, Conrad R, Strunk H, Hoogeveen R, von Falkenhausen M, et al. Randomly segmented central k-space ordering in high-spatial-resolution contrast-enhanced MR angiography of the supraaortic arteries: initial experience. Radiology. 2002; 225:583–588. [PubMed: 12409598]
14. Koenigkam-Santos M, Sharma P, Kalb B, Carew J, Oshinski JN, Martin D. Lower extremities magnetic resonance angiography with blood pressure cuff compression: quantitative dynamic analysis. J Magn Reson Imaging. 2009; 29:1450–1456. [PubMed: 19472421]
15. Zhang HL, Ho BY, Chao M, Kent KC, Bush HL, Faries PL, et al. Decreased venous contamination on 3D gadolinium-enhanced bolus chase peripheral MR angiography using thigh compression. AJR. 2004; 183:1041–1047. [PubMed: 15385302]
16. Pruessmann KP, Weiger M, Scheidegger MB, Boesiger P. SENSE: sensitivity encoding for fast MRI. Magn Reson Med. 1999; 42:952–962. [PubMed: 10542355]
17. Weiger M, Pruessmann KP, Boesiger P. 2D SENSE for faster 3D MRI. Magma. 2002; 14:10–19. [PubMed: 11796248]
18. Griswold MA, Jakob PM, Heidemann RM, Nittka M, Jellus V, Wang J, et al. Generalized autocalibrating partially parallel acquisitions (GRAPPA). Magn Reson Med. 2002; 47:1202–1210. [PubMed: 12111967]
19. Roemer PB, Edelstein WA, Hayes CE, Souza SP, Mueller OM. The NMR phased array. Magn Reson Med. 1990; 16:192–225. [PubMed: 2266841]
20. Haider CR, Glockner JF, Stanson AW, Riederer SJ. Peripheral vasculature: high-temporal- and high-spatial-resolution three-dimensional contrast-enhanced MR angiography. Radiology. 2009; 253:831–843. [PubMed: 19789238]
21. Johnson CP, Haider CR, Borisch EA, Glockner JF, Riederer SJ. Time-resolved bolus-chase MR angiography with real-time triggering of table motion. Magn Reson Med. 2010; 64:629–637. [PubMed: 20597121]
22. Mostardi PM, Young PM, McKusick MA, Riederer SJ. High temporal and spatial resolution imaging of peripheral vascular malformations. J Magn Reson Imaging. 2012:n/a–n/a.
23. Nael K, Fenchel M, Krishnam M, Laub G, Finn JP, Ruehm SG. High-spatial-resolution whole-body MR angiography with high-acceleration parallel acquisition and 32-channel 3.0-T unit: initial experience. Radiology. 2007; 242:865–872. [PubMed: 17325071]
24. Hardy CJ, Darrow RD, Saranathan M, Giaquinto RO, Zhu Y, Dumoulin CL, et al. Large field-of-view real-time MRI with a 32-channel system. Magn Reson Med. 2004; 52:878–884. [PubMed: 15389946]
25. Weavers PT, Borisch EA, Johnson CP, Riederer SJ. Acceleration apportionment: A method of improved 2D SENSE acceleration applied to 3D contrast-enhanced MR angiography. Magn Reson Med. 2013; 71:672–680. [PubMed: 23450817]
26. Breuer FA, Blaimer M, Mueller MF, Seiberlich N, Heidemann RM, Griswold MA, et al. Controlled aliasing in volumetric parallel imaging (2D CAIPIRINHA). Magn Reson Med. 2006; 55:549–556. [PubMed: 16408271]
27. Weavers PT, Borisch Ea, Riederer SJ. Selection and evaluation of optimal two-dimensional CAIPIRINHA kernels applied to time-resolved three-dimensional CE-MRA. Magn Reson Med. 2014; 73:2234–2242. [PubMed: 25046590]
28. Fronek A, Coel M, Berstein EF. Quantitative ultrasonographic studies of lower extremity flow velocities in health and disease. Circulation. 1976; 53:957–960. [PubMed: 1269131]

29. Haider CR, Hu HH, Campeau NG, Huston J 3rd, Riederer SJ. 3D high temporal and spatial resolution contrast-enhanced MR angiography of the whole brain. Magn Reson Med. 2008; 60:749–760. [PubMed: 18727101]
30. Haider CR, Riederer SJ, Borisch EA, Glockner JF, Grimm RC, Hulshizer TC, et al. High temporal and spatial resolution 3D time-resolved contrast-enhanced magnetic resonance angiography of the hands and feet. J Magn Reson Imaging. 2011; 34:2–12. [PubMed: 21698702]
31. Mostardi PM, Glockner JF, Young PM, Riederer SJ. Contrast-enhanced MR angiography of the abdomen with highly accelerated acquisition techniques. Radiology. 2011; 261:587–597. [PubMed: 21900616]
32. Weavers, PT.; Borisch, EA.; Johnson, CP.; Riederer, SJ. Acceleration Apportionment for Patient-Specific SENSE-Accelerated 3D CE-MRA. Proc 20th Annu. Meet. ISMRM; Melbourne, Victoria, Australia. 2012. p. 2224
33. Kellman P, McVeigh ER. Image reconstruction in SNR units: a general method for SNR measurement. Magn Reson Med. 2005; 54:1439–1447. [PubMed: 16261576]
34. Weavers, PT.; Cline, CC.; Johnson, CP.; Rossman, PJ.; Hulshizer, TC.; Riederer, SJ. A 16 Element Phased Array Surface Coil for Time-Resolved CE-MRA at SENSE Accelerations up to 12. Proc 20th Annu. Meet. ISMRM; Melbourne, Victoria, Australia. 2012. p. 2648
35. Johnson CP, Polley TW, Glockner JF, Young PM, Riederer SJ. Buildup of image quality in view-shared time-resolved 3D CE-MRA. Magn Reson Med. 2013; 70:348–357. [PubMed: 22936574]
36. Hardy CJ, Giaquinto RO, Piel JE, Rohling AASKW, Marinelli L, Blezek DJ, et al. 128-channel body MRI with a flexible high-density receiver-coil array. J Magn Reson Imaging. 2008; 28:1219–1225. [PubMed: 18972330]
37. Berglund J, Ahlström H, Johansson L, Kullberg J. Two-point dixon method with flexible echo times. Magn Reson Med. 2011; 65:994–1004. [PubMed: 21413063]
38. Stinson EG, Trzasko JD, Weavers PT, Riederer SJ. Dixon-type and subtraction-type contrast-enhanced magnetic resonance angiography: A theoretical and experimental comparison of SNR and CNR. Magn Reson Med. 2014:n/a–n/a.
39. Eggers H, Brendel B, Duijndam A, Herigault G. Dual-echo Dixon imaging with flexible choice of echo times. Magn Reson Med. 2011; 65:96–107. [PubMed: 20860006]
40. Leiner T, Habets J, Versluis B, Geerts L, Alberts E, Blanken N, et al. Subtractionless first-pass single contrast medium dose peripheral MR angiography using two-point Dixon fat suppression. Eur Radiol. 2013; 23:2228–2235. [PubMed: 23591617]

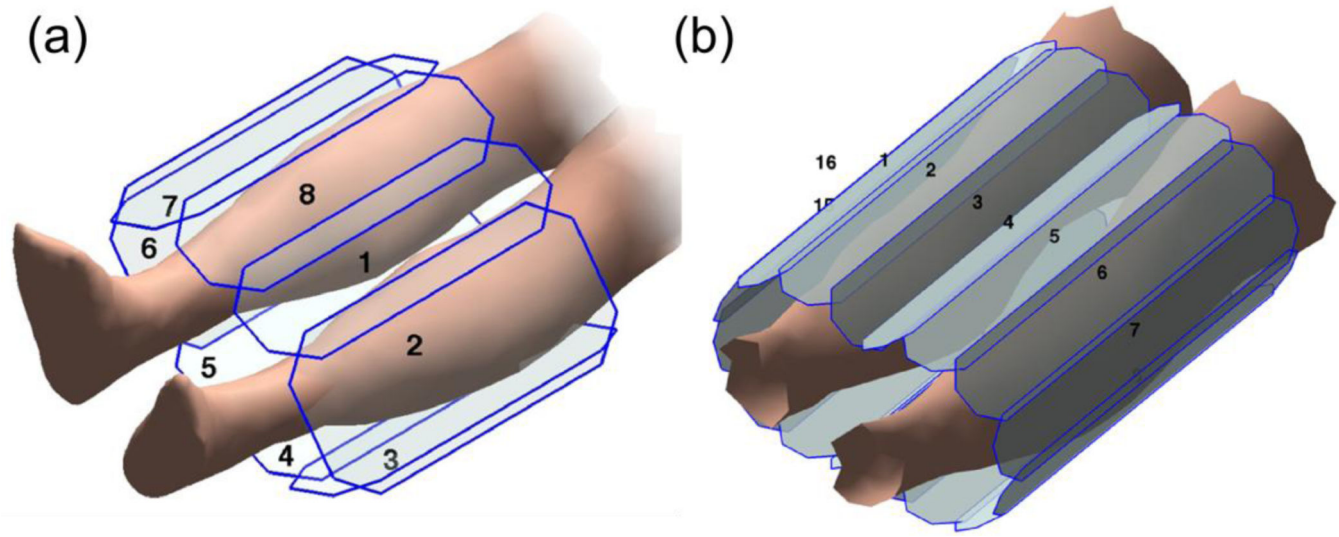

Figure 1.

A comparison of coil schematics of the previous (a) 8 element receiver coil capable of acceleration $R_Y \times R_Z = 4 \times 2 = 8$ and new (b) 16 element receiver capable of $R_Y \times R_Z = 6 \times 2 = 12$. Note the increased receiver count and shape tailored to the calf anatomy. Additionally, the S/I extent is increased from 27cm to 40cm.

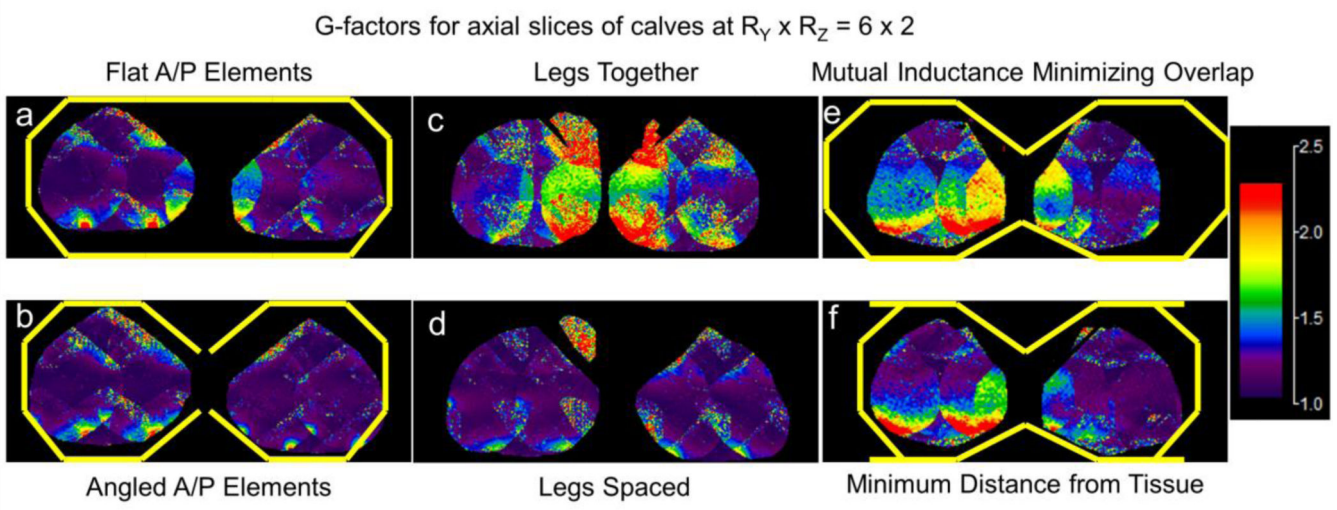

Figure 2.

A set of axial slices in the 3D g-factor map for a simulated 12× 2D-SENSE acceleration with various receiver coil configurations. Panels (a,b) compare the positioning of the anterior and posterior element configurations, either flat across the top and bottom (a) or angled in toward the center of the calves (b). The angled elements produced g-factor maps with lower values. Panels (c,d) compare the spacing between or outside of the legs, note reduced g-factor values in the panel with the spaced legs (d). Panels (e,f) compare configuration in which either (e) the nearest neighbor receiver coil overlaps that minimize mutual inductance are respected causing increased coil-to-subject lateral air gapor (f) the receivers are placed such that they are as close to the tissue as possible. Note it is more advantageous to locate the receivers close to the tissue (f) vs. minimizing mutual inductance.

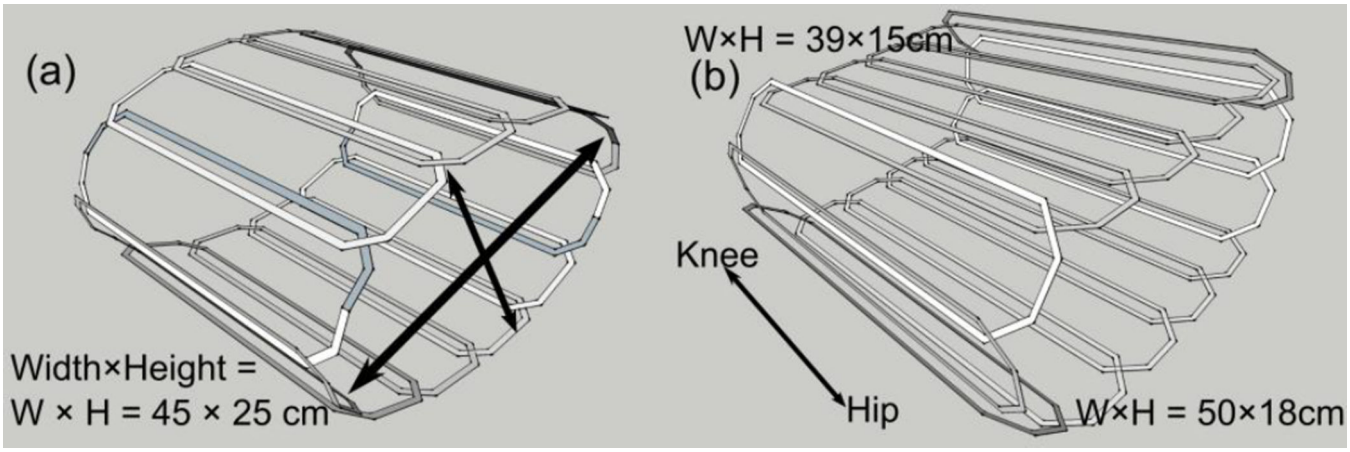

Figure 3.

A comparison of the previous (a) 12 element and new (b) 14 element thigh receiver arrays. Note the uniform elliptical cross-section in the previous array, causing an increased coil-to-subject gap at the knees. The new tapered receiver array with progressively changing cross-sectional area, allows for a tighter fit at the knees while at the same time allowing for a wider fit at the hips.

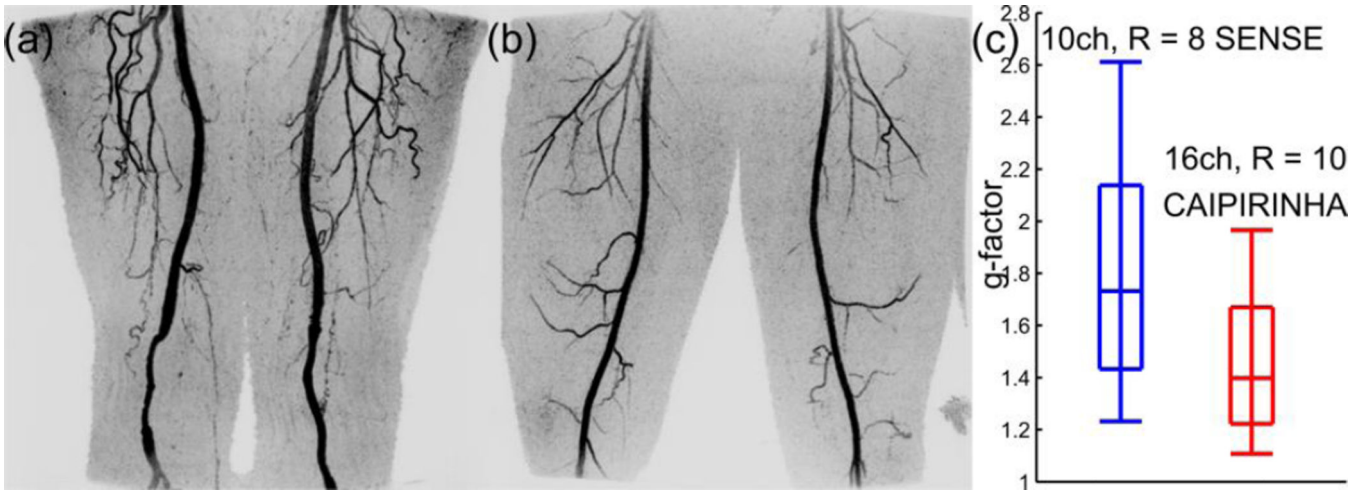

Figure 4.

Panels (a,b) compare the previous 12 channel thigh array at $R_Y \times R_Z = 4 \times 2$ and the new tapered thigh array at $R_Y \times R_Z$ (Shift) = 1 × 10 (7). Note the wider hip-facing area (50cm wide) and the narrower knee facing area (39cm wide). This allows the receiver elements to fit closer to the tissue. Panels (c,d) compare coronal MIPs from comparable contrast enhanced CE-MRA volunteers. Note also that the R = 10 accelerated g-factors in the 16 channel case are lower than the R = 8 accelerated g-factors in the 10 channel case shown in panel (e).

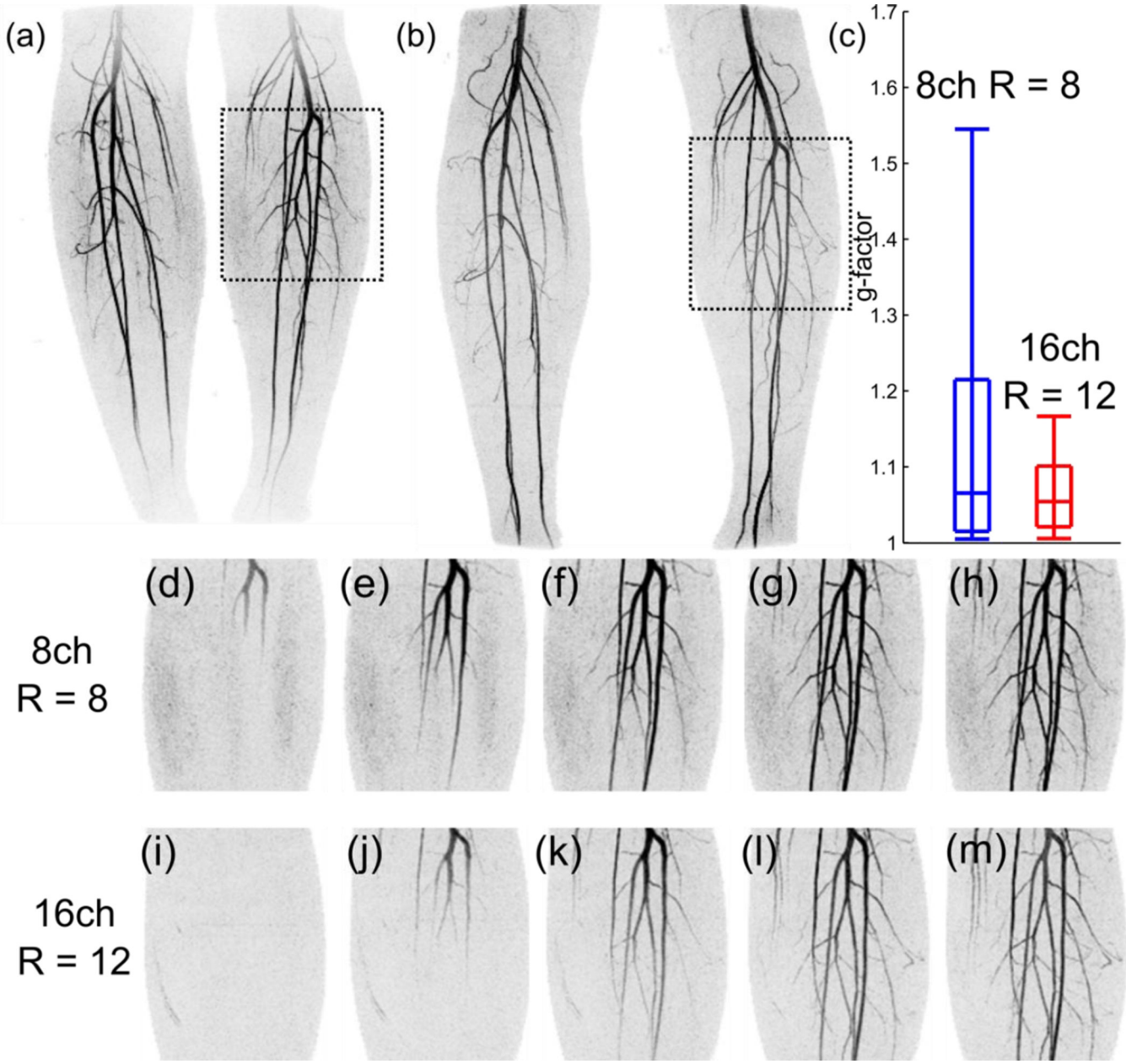

Figure 5.

Panels (a,b) show coronal MIPs from a time-resolved 3D CE-MRA of the same volunteer. Note reduced noise amplification along with better S/I coverage. Panel (c) shows the g-factor statistics (10^{th}, 25^{th}, median, 75^{th}, and 90^{th} percentiles denoted by box-and-whiskers) from the given 3D g-factor volume associated with the generation of the MIPs in the rest of the figure. Note that the R = 12 accelerated g-factors are lower in the 16 channel case when compared to the R = 8 accelerated g-factors in the 8 channel case. Panels (d–m) show a comparison of the indicated sections in (a,b) though time, from arrival of the contrast agent through the late arterial phase images.

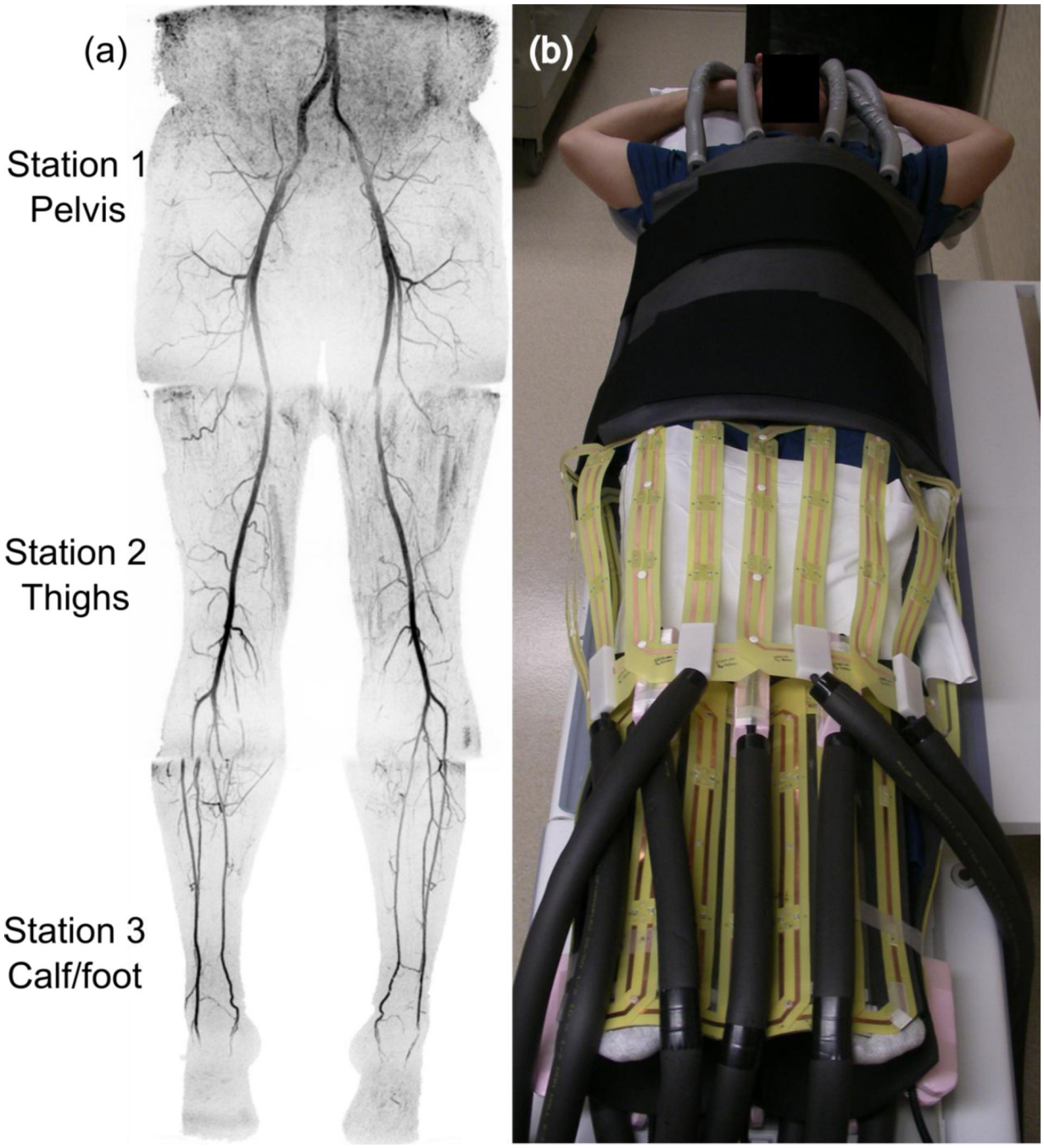

Figure 6.

Three-station MIP of a volunteer showing the last frame each of the pelvic and station, along with the second frame in the calves. Absence of venous overlay speaks to the effectiveness of the combination of high parallel imaging acceleration and interactive tracking and triggering. Panel (b) shows how the receiver array fits on a volunteer, different from that imaged in (a). CAIPIRINHA parameters for the pelvic and thigh stations were $R_Y \times R_Z = 2 \times 4$ (2) and $R_Y \times R_Z = 2 \times 5$ (2). Acceleration in the calves was apportioned as $R_Y \times R_Z = 4.42 \times 2.75 = 12.16$.

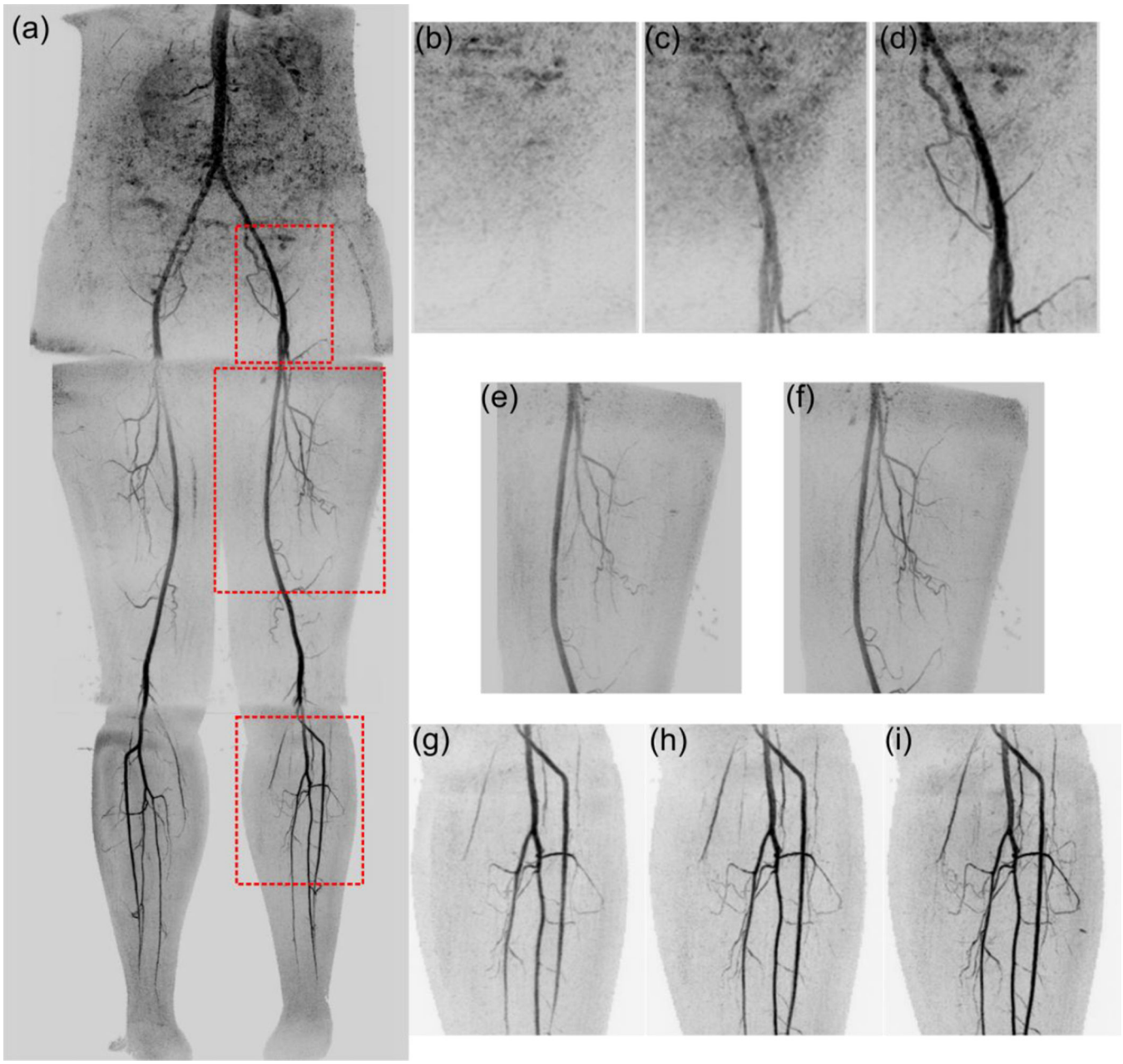

Figure 7.

Three-station MIP of a second volunteer is shown (a), along with various zoomed in sections from the time series of the acquisition. The final three MIPs from the pelvic station are shown in (b,c,d). The only two time frames of the thighs are shown in (e,f), and the first three time frames in the calves are shown in (g,h,i). In particular panels (e,f) show how even with just 2.1 and 4.2 seconds of data acquisition, high quality arteriograms of the small vessels in the thigh can be formed on the way to acquiring a distal station. CAIPIRINHA parameters for the pelvic and thigh stations were $R_Y \times R_Z = 1 \times 8$ (6) and $R_Y \times R_Z = 1 \times 10$ (8). Acceleration in the calves was apportioned as $R_Y \times R_Z = 4.48 \times 2.75 = 12.32$.

Table 1

Acquisition parameters; both for single station coil array comparison scans and for 3-station fluoroscopically tracked and triggered CE-MRA volunteers. “Previous” indicates parameters reported in Johnson, et al, [8] whereas “New” indicates parameters used in this work.

Parameter Table: Station	Abdomen-Pelvis	Thighs	Calves-Feet
FOV (cm: S/I × L/R × A/P)	42 × 42 × 14.4	42 × 42 × 13.2	42 × 33.6 × 13.2
Sampling Matrix (S/I × L/R × A/P)	280 × 280 × 96	280 × 280 × 88	420 × 336 × 132
Resolution (mm: S/I × L/R × A/P)	1.5 × 1.5 × 1.5	1.5 × 1.5 × 1.5	1.0 × 1.0 × 1.0
Flip Angle (°)	30	30	30
Bandwidth (kHz)	±62.5	±62.5	±62.5
TR / TE (ms)	4.6 / 2.0	4.6 / 2.0	5.8 / 2.7
Receiver Coil # - Previous	12–14	10	8
Receiver Coil # - New	**16**	**14–16**	**16**
View Sharing Sequence	N3 CAPR	N3 CAPR	N4 CAPR
2D-SENSE Acceleration - Previous	R=8 (4×2)	R=8 (4×2)	R=8 (4×2)
2D-SENSE Acceleration - New	**R=8 (CAIPIRINHA)**	**R=10 (CAIPIRINHA)**	**R=12 (Apportioned)**
2D Partial Fourier Acceleration	1.9	1.9	1.8
Frame Time (sec) – Previous	2.5	2.5	5.2
Temporal Footprint (sec) - Previous	6.8	6.8	18.7
Frame Time (sec) – New	**2.5**	**2.1**	**4.0**
Temporal Footprint (sec) - New	**6.8**	**5.7**	**13.9**